Acta Cryst. (1974). A30, 316

A Coherent Elastic Model for the Determination of the Orientation of Exsolution Boundaries: Application to the Feldspars

BY C. WILLAIME* AND W. L. BROWN†

Laboratoire de Minéralogie Cristallographie, associé au C.N.R.S., Université Paris VI, 4 *Place Jussieu*, 75230 *Paris–Cedex* 05, *France*

(*Received* 29 *May* 1973; *accepted* 25 *November* 1973)

On the basis of proposals by Cahn [*Acta Met.* (1962). **10**, 179–183] for cubic crystals, a coherent elastic model is developed which makes it possible for the orientations of exsolution boundaries formed either by spinodal decomposition or homogeneous nucleation to be predicted. The elastic energy for the coherent exsolution boundary is calculated for all orientations of the boundary, the minimum value for this energy corresponding to the predicted boundary. A program has been written which can be applied to all crystal systems; it uses as input the lattice parameters of crystals having the same compositions as the exsolution domains and their corresponding elastic stiffnesses. The approximations of the model are discussed, especially the neglect of relaxation of the coherence stresses away from the boundary, and the uncertainties in the calculated results due to errors in or lack of knowledge of the input data. The coherent elastic model has been used to determine the orientations of exsolution boundaries in the feldspars. The agreement between calculated and observed exsolution boundaries is remarkable, considering that room-temperature lattice parameters and elastic stiffnesses are used. The angular differences are less than 3° in most cases. They may reach 20° in the labradorites because the input data are not well known. All observed exsolution boundaries have been accounted for and some unknown ones calculated. The results of the calculations may be used to explain the cause of the exsolution orientations and to suggest areas requiring further research.

I. Introduction

Crystals are frequently not homogeneous, and one of the common inhomogeneities is exsolution, especially in minerals and metals. The exsolution phenomenon may produce domains of different or practically identical atomic structure. This paper deals with the latter case, in which a homogeneous crystal gives rise to two kinds of domain which differ only slightly in composition and in lattice parameters. For exsolution to take place, it is necessary that certain atoms or groups of atoms can diffuse through the crystal without modifying the structure except for slight variations in the atomic coordinates due to differences in the sizes of the atoms.

Two mechanisms are possible, homogeneous nucleation and spinodal decomposition. Right from the start of homogeneous nucleation, the diffusion produces a sharp change in composition at the domain boundaries and the domains are of limited extent. At the beginning of spinodal decomposition, on the other hand, the domains differ infinitesimally in composition but extend throughout the crystal.

In both cases, reaction proceeds in such a way as ultimately to achieve a minimum in free energy. The boundaries between domains will involve a certain amount of elastic energy; if this energy varies with the orientation of the boundary, the total free energy will be minimized when the boundary energy is a minimum. Except in glasses, exsolution boundaries are nearly planar and have a definite orientation in almost all cases. The exsolution textures markedly affect the physical properties of the crystal and also contain valuable information about its past history. The object of this paper is to propose a method for calculating the boundary elastic energy between coherent or essentially coherent domains in order to determine the optimal orientation of the boundary. This method will be compared with the optimal-phase-boundary model of Bollmann (Bollmann, 1970; Bollmann & Nissen, 1968) and applied to a problem of particular interest and complexity – the exsolution relations in the feldspars, a mineral group of triclinic or monoclinic symmetry.

II. Coherent elastic boundary model

1. *Theory of the calculation of the boundary elastic energy*

During a study of the energy involved in spinodal decomposition of a solid, Cahn [for a review, see Cahn (1968)] defined the elastic energy of the boundaries between domains with a view to calculating the coherent spinodal curve with respect to the chemical spinodal curve. He formulated this boundary elastic energy in the case of an isotropic solid (Cahn, 1961) and in that of a cubic solid (Cahn, 1962). We have adopted the simple totally coherent hypotheses of

* This work constitutes part of a Doctorat d'Etat ès-Sciences from the University of Paris (CNRS Thesis number AO 7172).

† Present address: Laboratoire de Minéralogie, Université de Nancy I, Case officielle 140, 54037 Nancy Cedex, France.

Cahn and have generalized them to the case of a crystal of any symmetry.

The elastic boundary energy W^E is given by $W^E = \frac{1}{2}\mathbf{S}^E_\alpha \mathbf{T}_\alpha$ where the $\mathbf{S}^E_\alpha$ are the elastic strain tensor components imposed on the lattice to permit coherence along the boundary and the $\mathbf{T}_\alpha$ are the corresponding stress tensor components. To evaluate the various components, it is necessary to define a total strain tensor $\mathbf{S}^T$ and a compositional strain tensor $\mathbf{S}^N$ due to the variation in composition ΔN, and to adopt several hypotheses.

The quantity to be calculated is the boundary elastic energy for any orientation of the planar boundary between two exsolution domains. An orthogonal axial system OX_1, OX_2, OX_3 is chosen such that OX_3 is perpendicular to the boundary plane, OX_1 and OX_2 being in this plane.

To simplify the calculations, it is supposed that the exsolution domains are of equal volume. Thus if $N(0)$ is the molar fraction of one of the components before exsolution, the corresponding values after exsolution in domains 1 and 2 are

$$N(1) = N(0) + \Delta N \text{ and } N(2) = N(0) - \Delta N .$$

(a) First postulate of the model

The lattice is completely coherent along the boundary plane OX_1X_2 and there is no deformation of these parallel planes anywhere in the crystal during the exsolution (Cahn, 1962). $\mathbf{S}^T$ is the total strain tensor between the lattice before and after exsolution, and its components parallel to the OX_1X_2 plane are zero. Hence:

$$\mathbf{S}^T_{11} = \mathbf{S}^T_{22} = \mathbf{S}^T_{12} = 0 . \qquad (1a)$$

It is convenient to express this alternatively in Voigt's notation in which it becomes

$$\mathbf{S}^T_1 = \mathbf{S}^T_2 = \mathbf{S}^T_6 = 0 . \qquad (1b)$$

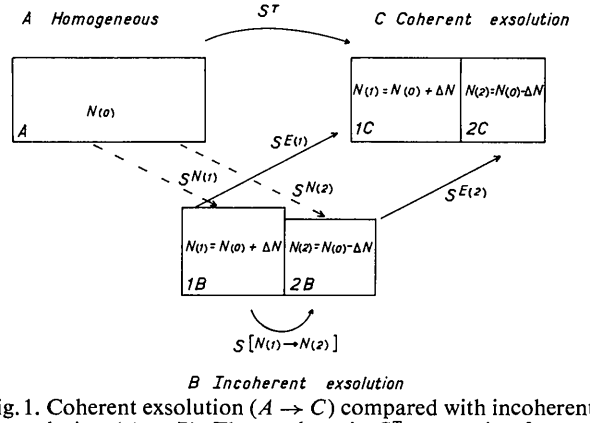

Fig. 1. Coherent exsolution ($A \rightarrow C$) compared with incoherent exsolution ($A \rightarrow B$). The total strain S^T on passing from A to C can be decomposed into a compositional strain S^N caused by a change in composition ΔN ($A \rightarrow B$) and an elastic strain S^E required to restore coherency ($B \rightarrow C$). The lattice can have any given orientation compared to the coherent boundary OX_1X_2.

Coherent exsolution according to this model is shown in Fig. 1 by the process $A \rightarrow C$ where A is homogeneous and of composition $N(0)$ and C represents the two domains of composition $N(1)$ and $N(2)$. $\mathbf{S}^T$ is the total strain tensor on passing from lattice A to lattice $1C$.

In order to carry out the calculations, it is supposed that the passage from A to C is broken up into two parts by way of B (Fig. 1), in which the two domains have the same compositions $N(1)$ and $N(2)$ as in C but are in simple contact along the plane OX_1X_2 without any coherence. The two domains $1B$ and $2B$ have normal unstressed lattice parameters, the situation corresponding on a macroscopic scale to incoherent two-phase exsolution, but without any interaction on the boundary.

The compositional strain tensors $\mathbf{S}^{N(1)}$ and $\mathbf{S}^{N(2)}$ describe the passage from lattice A to lattice $1B$ and to lattice $2B$ respectively. The passage from lattice $1B$ to lattice $2B$ is described by the tensor $\mathbf{S}^{[N(1) \rightarrow N(2)]}$ which we will call the compositional-misfit tensor.

It is obvious that

$$\mathbf{S}^{[N(1) \rightarrow N(2)]} = -\mathbf{S}^{N(1)} + \mathbf{S}^{N(2)} .$$

Since the strains produced by small differences in composition $+\Delta N$ and $-\Delta N$ are equal and opposite, it follows that

$$\mathbf{S}^{N(1)} = -\mathbf{S}^{N(2)} .$$

Then we may write

$$\mathbf{S}^N \equiv \mathbf{S}^{N(1)} \equiv -\mathbf{S}^{N(2)} = -\tfrac{1}{2}\mathbf{S}^{[N(1) \rightarrow N(2)]}$$

The components of $\mathbf{S}^{[N(1) \rightarrow N(2)]}$ can be calculated directly from the unstressed lattice parameters of homogeneous macroscopic crystals of compositions $N(1)$ and $N(2)$.

The passage from B to C (Fig. 1) requires an elastic deformation to obtain coherence on the plane OX_1X_2. For this $\mathbf{S}^E$ is the elastic strain tensor, $\mathbf{S}^{E(1)}$ for domain 1 and $\mathbf{S}^{E(2)}$ for domain 2. For small strains

$$\mathbf{S}^{E(1)} = -\mathbf{S}^{E(2)} = \mathbf{S}^E .$$

The total strain tensor $\mathbf{S}^T$ is the sum of the two parts due to the change in composition $\mathbf{S}^N$ and to the elastic deformation $\mathbf{S}^E$; hence

$$\mathbf{S}^T = \mathbf{S}^N + \mathbf{S}^E . \qquad (2)$$

If $\mathbf{T}$ is the stress tensor related to the elastic strain, the boundary elastic energy per unit volume is, in Voigt's notation

$$W^E = \tfrac{1}{2}\mathbf{S}^E_\alpha \mathbf{T}_\alpha \quad (\alpha = 1 \text{ to } 6) . \qquad (3)$$

(b) Second postulate of the model

There are no stresses opposing a deformation perpendicular to the boundary plane at any point in the crystal (Cahn, 1962). This implies that the components perpendicular to the boundary plane of the stress

tensor **T** which produces the elastic deformation of the crystal are zero:

$$\mathbf{T}_{33}=\mathbf{T}_{32}=\mathbf{T}_{31}=0 \qquad (4a)$$

or, in Voigt's notation

$$\mathbf{T}_3=\mathbf{T}_4=\mathbf{T}_5=0\,. \qquad (4b)$$

The relation of the components of $\mathbf{S}^E$ and **T** is given, in Voigt's notation, by

$$\mathbf{T}_\alpha=c_{\alpha\beta}\mathbf{S}^E_\beta \quad (\alpha,\beta=1 \text{ to } 6) \qquad (5)$$

where $c_{\alpha\beta}$ are the elastic stiffness coefficients expressed in the same axial system $OX_1X_2X_3$ as are the components of $\mathbf{S}^E$ and **T**. This relation provides six equations which allow the calculation of the six unknown components in the tensors $\mathbf{S}^E$ and **T**; since, of the other six components, $\mathbf{T}_3$, $\mathbf{T}_4$ and $\mathbf{T}_5$ are zero from equation (4) (a consequence of postulate 2), and $\mathbf{S}^E_1$, $\mathbf{S}^E_2$ and $\mathbf{S}^E_6$ are known from the following argument. Equation (1) gives

$$\mathbf{S}^T_1=\mathbf{S}^T_2=\mathbf{S}^T_6=0$$

and if equation (2) is written in terms of its components,

$$\mathbf{S}^T_\alpha=\mathbf{S}^N_\alpha+\mathbf{S}^E_\alpha\,,$$

it follows that

$$\mathbf{S}^E_1=-\mathbf{S}^N_1 \quad \mathbf{S}^E_2=-\mathbf{S}^N_2 \text{ and } \mathbf{S}^E_6=-\mathbf{S}^N_6\,.$$

It is thus possible to calculate all the terms in equation (3) and obtain the value of the coherent elastic energy for each successive orientation of the boundary plane OX_1X_2.

The chief difficulty is that the necessary input information is expressed in axial systems which differ from one another and from that used in the above formal treatment, and must be transformed to be consistent with one another. The calculated orientation must also be transformed to an axial system in which it can be compared with experimental results. The method of doing so is described in the next section.

2. *Outline of the program for calculating the boundary elastic energy*

Several axial systems must be defined for the calculations:

- Axial system (1): crystallographic system corresponding to crystal 1 (in general non-orthogonal).
- Axial system (2): crystallographic system corresponding to crystal 2.
- Axial system (3): an average axial system, intermediate between the above two; the angular and unit vector values are obtained by taking the half sum of the corresponding values in systems 1 and 2.
- Axial system (4): the orthogonal system OZ_1, OZ_2, OZ_3 in which the elastic stiffness coefficients are given. For monoclinic and triclinic feldspar crystals OZ_3 coincides with **c***, OZ_2 with **b**, and OZ_1 is normal to the other two.
- Axial system (5): the orthogonal system OY_1, OY_2, OY_3 normally used for stereographic projections. OY_3 coincides with **c**, OY_2 with **b***, and OY_1 is normal to the other two. In this system a direction is defined by its direction cosines m_1, m_2 and m_3 or by its polar angles φ and ϱ where $\cos\varrho=m_3$ and $\tan\varphi=m_1/m_2$.
- Axial system (6): Orthogonal system OX_1, OX_2, OX_3 defined in the previous section and related to the orientation of the boundary plane. OX_3 is normal to this plane and the axes OX_1 and OX_2 lie anywhere in the plane.

The deformation of the lattice due to the variation in composition is calculated in system 4 from the projections on system 4 of the unit cell of domains 1 and 2, expressed initially in systems 1 and 2 respectively. This gives the misfit strain tensor in system 4. The elastic stiffness coefficients are initially given in system 4.

For a given pair of angular coordinates, φ, ϱ, in system 5, the corresponding orientation of a plane in system 6 is calculated, and hence the transformation matrix from system 4 to system 6 is derived. Using this, the stiffness coefficients and the components of $\mathbf{S}^N$ in system 6 are obtained. The calculations of the values of $\mathbf{T}_\alpha$ and $\mathbf{S}^E_\alpha$, and hence the boundary energy W^E, are carried out in this system, using equations (1) to (5).

The values of φ and ϱ are varied stepwise by a loop, to scan all orientations over a hemisphere.

The input for the program comprises

(1) a set of lattice parameters for each component
(2) the elastic stiffness coefficients $c_{\alpha\beta}$
(3) specification of the steps and limits for the values of φ and ϱ.

Its output is the boundary elastic energy for each specified orientation, and the description of the orientation in terms of crystallographic indices in axial system 3.

3. *Limitations of the coherent elastic model*

The limitations of the simple model are of two sorts, those which are inherent in the model and those which are due to lack of data. An inherent limitation of the model is the fact that it does not allow for relaxation of stresses away from the boundary. The accidental limitations of the model are due to the fact that in general the lattice parameters, the elastic stiffness coefficients and the compositions of the domains are not known for the conditions of formation of the exsolution. These two types of limitation will be dealt with separately in what follows.

(*a*) *Relaxation of stresses away from the boundary*

At the very beginning of unmixing by spinodal decomposition the diffraction spots are elongate perpendicular to the boundary plane (Cadoret & Delavignette, 1969; Owen & McConnell, 1971; Owen, 1973), indicat-

ing that there is no variation in the lattice parameters parallel to the boundary plane, variations occurring only in the direction normal to it. Thus at this stage postulates (1) and (2) proposed by Cahn and adopted by us are justified to a first approximation. The orientation of the boundary plane at the beginning of exsolution could be calculated rigourously with this model, if the unstressed lattice parameters and stiffness coefficients were known for the compositions $N(0) \pm \Delta N$ very close to the initial composition $N(0)$ at the temperature and pressure of the unmixing.

At a more advanced stage of unmixing, the lattice parameters are different within the domains in both the direction of the exsolution plane as well as normal to it. Coherence is generally maintained at the boundary between the domains, but the stresses are relaxed as the distance from the boundaries increases. As a result the unit cell of the lattice varies with position and tends to approach the unstressed state far from the boundaries. This relaxation can be shown to be similar to that observed near a dislocation network. When the exsolution lamellae are thin, the parameters inside each lamella of the same composition are nearly constant, because of partial relaxation of the stresses, and differ less from the parameters on the boundary than do the unstressed parameters (Brown & Willaime, 1973).

The schematic variation of R, a lattice parameter parallel to the boundary, as a function of distance from the boundary is shown in Fig. 2 by the curve $ABCDE$; P_1 and P_2 represent the normal unstressed parameters corresponding to domains 1 and 2, and A, C or E the parameter for the coherent model. According to the model the stored elastic energy is that for the passage P_1 to C in domain 1 and P_2 to C in domain 2. The simple model is only correct near the boundary. The stored elastic energy linked to exsolution with relaxation is that corresponding to the passage P_1 to R_1 and

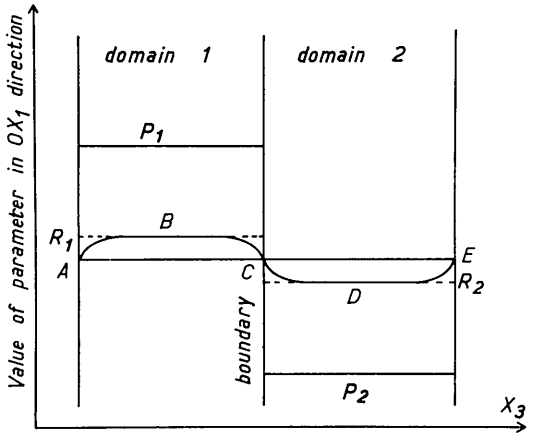

Fig. 2. The variation of the lattice parameter (along OX_1) as a function of the distance from the boundary along OX_3. R_1 and R_2 are the observed values of the parameter in domains 1 and 2 (after relaxation of the coherency stresses), C is the totally coherent parameter and P_1 and P_2 are the stress-free parameters.

P_2 to R_2. If the model were applied at all points using as initial parameters P_1 and P_2 and as final parameters R_1 and R_2 the real parameters at each point, it would be possible to calculate the stored elastic energy for the real crystal under relaxation. In fact, the simple model calculates the sum of the stored elastic energy and the energy liberated by relaxation of the stresses. The model should thus use undeformed parameters and not those measured after relaxation.

(*b*) *Estimates of the lattice parameters and elastic stiffnesses for condition of exsolution*

The calculation of the strains involves the *differences* between the unstressed parameters, and therefore their determination requires that the parameters themselves must be known with high precision. This is generally the case at room temperature but is less so at the high temperatures and/or pressures at which exsolution takes place. If the domains are very similar, both elastically and in composition, it is highly probable that the effects of temperature on both sets of parameters will also be similar and therefore the differences will keep their same *relative* values. In addition, an increase in hydrostatic pressure will to a first approximation reduce just those parameters which increase most readily with temperature, and therefore the two effects tend to oppose each other. The thermal strains produced by an increase in temperature of 1000 °C are generally of the order of a few percent and are often opposite to those produced by a hydrostatic pressure rise of the order of 20–40 kilobars at room temperature, (Clark, 1966). Since compressibility increases with increasing temperature, a smaller pressure increase would be necessary at 1000 °C to counterbalance the effect of the temperature rise.

The boundary elastic energy depends on the *average* values of the elastic stiffnesses, because the boundary energy is the half *sum* of the energies in unit volume on both sides of the boundary, the strains in the two domains being equal and opposite (when the domains are equal in size). The value for this energy will depend on the strains and the elastic stiffnesses. The stiffnesses decrease with increasing temperature, the decrease being of the order of several percent per 100 °C, and the increase in pressure needed to counterbalance this decrease is of the order of 3–5 kilobars for materials of average stiffness. As might be expected, the temperature and pressure coefficients $\left[\frac{1}{c}\left(\frac{\partial c}{\partial T}\right)\right.$ and $\left.\frac{1}{c}\left(\frac{\partial c}{\partial P}\right)\right]$ are greatest for the smallest stiffness coefficients, which correspond to the materials with largest thermal expansion and compressibility coefficients.

(*c*) *Effect of the composition and relative amounts of the domains*

The model proposed by Cahn for spinodal decomposition involves planar sinusoidal variations in composition. In order to calculate the elastic energy, it is necessary to choose two close compositions on either

side of the critical composition. Frequently, lattice parameters and elastic stiffness are only known for the extreme compositions and one must assume a linear relation between them and composition (or use the extreme compositions, which amounts to the same thing).

The parameters on the boundary plane will depend on the relative sizes of the two domains and will not be equal to the mean values of their parameters, unless the domains are equal in size. In fact, the differences between the parameters of the unstressed domain and those along the boundary plane will, to a first approximation, depend inversely on the relative sizes of the domains (Cahn, 1968; Brown & Willaime, 1973). The values of W will be unaffected by changes in the relative sizes of the domains if the elastic stiffnesses in the two domains are the same, and only slightly affected if the stiffnesses are different.

(d) Applicability of the simple coherent elastic model

At the beginning of this section, the limitations of the simple model were outlined; we have shown that these limitations are not likely to be serious if we are concerned only with *relative* values of the elastic boundary energies at different orientations, and this is all that is needed for predicting directions of their minima.

For low-symmetry materials this can provide a stringent test. In performing our calculations with room-temperature lattice parameters and stiffnesses, we are testing the validity of the approximations outlined in this section as well as of the model itself. A test of this kind is the application of the model to exsolution systems in the feldspars, to be described in § III below.

4. *Comparison with other boundary models*

The 0-lattice theory of Bollmann (1967, 1970) enables calculations to be made of the orientation of grain boundaries between crystals of the same composition but different orientations, and also of exsolution boundaries between lamellae of slightly different compositions in a composite crystal. With the introduction of an additional hypothesis, this leads to the optimal-phase-boundary model of Bollmann & Nissen (1968).

This latter method consists of allowing the two slightly different lattices to interpenetrate with a common lattice point and nearly parallel orientations. On slight rotation of the two lattices, coincidence of some of the lattice points (or in general of equivalent points in the unit cells) is sought, which gives rise to a multiple cell common to both lattices.

The smallest of these multiple cells is the unit cell of the 0-lattice. The composition plane of the two crystals occurs on one of the faces of the 0-lattice unit cell. Bollmann & Nissen indicated that the boundary was the site of a double array of dislocations. The three potential composition planes for each possible 0-lattice are arranged in order of their surface energy, the minimum energy corresponding to the exsolution plane. The value of the energy is not calculated, a parameter P being used instead which is supposed to vary in a monotonic fashion with the surface energy. This is defined by

$$P=\left(\frac{\mathbf{b}_1}{d_1}\right)^2+\left(\frac{\mathbf{b}_2}{d_2}\right)^2$$

where $\mathbf{b}_1$ and $\mathbf{b}_2$ are the Burgers vectors for the dislocation arrays of spacings d_1 and d_2.

The only input data needed for calculations using Bollmann's optimal-phase-boundary model are the unstressed lattice parameters corresponding to the compositions of the two crystals (no stiffness coefficients are needed, the medium being considered isotropic) and the output is the orientations of the two lattices and of the plane of best fit.

The two models are compared schematically in Fig. 3. Both models correspond only partly to the observed situation near the boundary. The weakness of the coherent elastic model is not to take into account the relaxation of the stresses away from the boundary (Fig. 3, *C* to *D*), though this may not substantially affect the orientation of the calculated composition plane (see previous section.) Its major advantage is that it allows for elastic anisotropy. If the exsolution took place by spinodal decomposition or by homogeneous nucleation, the simple coherent elastic model is justified provided the correct parameters and stiffnesses are used. Bollman & Nissen's model does not allow for coherence and should require that the exsolution take place by heterogeneous nucleation, the lattice of the nucleating phase being oriented relative to the host lattice by a dislocation network, the optimum fit corresponding to a minimum in its energy (or in the parameter P).

Bonnett & Durand (1972) proposed a different purely geometrical method for calculating the position of the boundary plane, following Bollmann's 0-lattice theory.

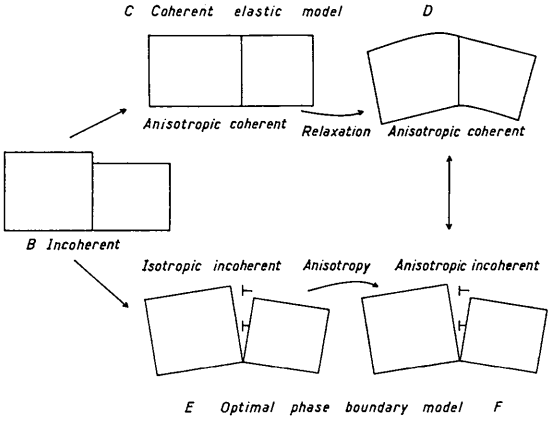

Fig. 3. Comparison of the coherent elastic model (*C*) and the optimal-boundary model (*E*). It is probable that the real state of the boundary is partial coherency between states *D* and *F*.

They calculated the pure strain on passing from one lattice to the other, as represented by the quadric associated with the strain tensor. It is always possible to reduce the problem to one of two cases:

(1) The pure strain coefficients ε_1, ε_2 and ε_3 parallel to the principal axes of the quadric have the same sign – the quadric is an ellipsoid and the plane of minimum deformation (assumed to be the boundary plane) is that containing the two axes with the smallest strain coefficients, ε_2 and ε_3.

(2) Two of the principal pure strain coefficients are positive ε_1 and ε_2 with $\varepsilon_1 > \varepsilon_2$ and the third is negative – the associated quadric is a one-sheet hyperboloid. The planes of minimum strain (the boundary planes) contain the principal axis of the quadric parallel to ε_2 and one of the directions of zero strain between ε_1 and ε_3. There are thus two planes of minimum strain symmetrically situated with regard to the plane ε_1 ε_2 (and ε_2 ε_3).

The parameter P defined by Bollmann & Nissen (1968) thus becomes

$$P=(\varepsilon')^2+(\varepsilon'')^2$$

where $\varepsilon'=\varepsilon_2$ and $\varepsilon''=\varepsilon_3$ in the first case and $\varepsilon'=0$ and $\varepsilon''=\varepsilon_2$ in the second case.
In our notation

$$P=(\mathrm{S}_1^N)^2+(\mathrm{S}_2^N)^2=(\mathrm{S}_1^E)^2+(\mathrm{S}_2^E)^2$$

where the axes OX_1 and OX_2 in the boundary plane are oriented such that S_6^E is zero. The elastic boundary energy is then given by

$$W^E=\tfrac{1}{2}\sum_{\alpha,\beta} c_{\alpha\beta}\mathrm{S}_\alpha^E\,\mathrm{S}_\beta^E \text{ with } \alpha=1,2 \quad \beta=1,2,3,4,5.$$

The terms containing S_1^E and S_2^E (those appearing in P) are generally the most important. It is clear that when the deformation needed to pass from lattice 1 to lattice 2 is nearly isotropic, the multiplication of the strain terms by the stiffness coefficients (generally unequal) will produce an inequality in energy for the same strain in different directions. The purely geometrical model will only work well when the strain is very anisotropic.

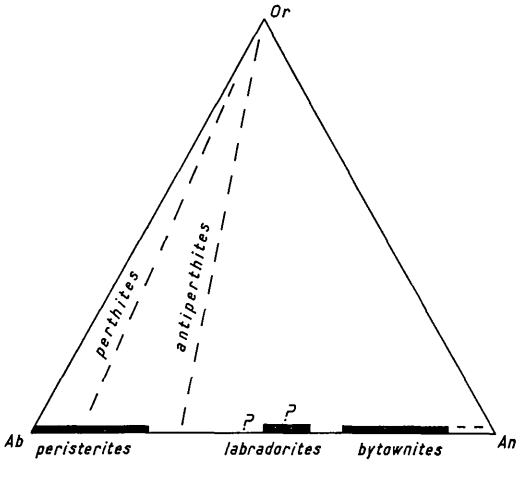

Fig. 4. The compositions of the different exsolution types in the feldspars.

III. Application of the coherent elastic boundary model to the feldspars

1. *Introduction*

The feldspars form the most highly studied mineral group. They are tectosilicates of monoclinic or triclinic symmetry. Those of interest here lie within the composition triangle whose corners are $KAlSi_3O_8$ (K-feldspar), $NaAlSi_3O_8$ (albite), and $CaAl_2Si_2O_8$ (anorthite). They show exsolution phenomena ranging from coarse scale to very fine scale, often associated with a beautiful iridescence in visible light. The exsolutions fall into three broad categories: those in the alkali feldspars (K, Na series) known as the *perthites*; those in the plagioclases (Na, Ca series) known according to composition range as *peristerites*, *labradorites*, and *bytownites*; and those in the more general composition range (Na, Ca, K) known as *antiperthites*. The last named will not be considered here, since not enough is known about them experimentally. The composition ranges are shown in Fig. 4.

Feldspars of given composition can differ in their state of Si, Al order, and this can affect their lattice parameters. In the alkali feldspars it can result in inversions between monoclinic and triclinic symmetry, occurring at about 600–900 °C, commonly associated with the production of twin textures. Thus, K-feldspars may be monoclinic [sanidine and orthoclase (totally or highly disordered)] or triclinic [intermediate microcline, (low obliquity and moderate ordering) and maximum microcline (high obliquity and total ordering)]. High albite and low albite are both triclinic at room temperature. The albites and microclines tend to twin in ways which imitate monoclinic symmetry (Albite law, Pericline law, and the superposition of both which gives 'cross-hatched microcline'). Such effects occur not only in homogeneous alkali feldspars but in the exsolution domains in the perthites; in this case the twinning reduces the strain energy along the boundary between a monoclinic and a triclinic domain (Willaime & Gandais, 1972). Twinning does not occur in exsolution textures in the plagioclases, which are all triclinic.

The perthites have been given descriptive adjectives or prefixes according to their different observed characteristics. We shall ignore these until a later section, when those relevant for our purposes will be defined.

The exact mechanism of the exsolution is not known in all cases, but is generally considered to occur by spinodal decomposition or homogeneous nucleation (Owen & McConnell, 1971; McConnell, 1973; Owen, 1973; Smith, 1972). The exsolution textures are lamellar and are essentially coherent. Isolated dislocations may occur along the boundaries with a periodicity in one case of the order of 1μm (Aberdam & Kern,

1962; Aberdam, 1965), but they in no sense form a dislocation network. Generally, two sets of lattice parameters exist for the two domains, indicating that relaxation has occurred away from the boundary. When the lamellae are less than about 1 μm thick the sets of lattice parameters for the two domains are strained (Laves, 1952; Smith, 1961; Wright & Stewart, 1968; Brown & Willaime, 1973; Viswanathan, 1968, 1973; Korekawa, Nissen & Philipp, 1970). In the case of the labradorites only one set of spots occurs suggesting that the two domains have the same lattice parameters (Nissen, Eggmann & Laves, 1967).

2. *Input data*

Accurate measurements neither of lattice parameters of the actual exsolution domains [according to § II.3(a) would they not be the best choice] nor of elastic stiffnesses are generally available. It is therefore necessary to match the domains against similar homogeneous feldspars for which the measurements are available. This requires a knowledge of the character of the domains, their composition, state of order, and twinning. The problems concerning these are of a different nature for the perthites and the plagioclase exsolutions.

Table 1. *Lattice parameters used in the calculations*

	Mineral name	Bulk composition Or	Ab	An	Parameters a (Å)	b (Å)	c (Å)	α (°)	β (°)	γ (°)	Reference
1	Synthetic sanidine	100	0	0	8·603	13·021	7·178	90	116·01	90	[9]
2	Synthetic sanidine	59	31	0	8·425	12·999	7·167	90	116·09	90	[9]
2	Synthetic sanidine	39	61	0	8·320	12·977	7·159	90	116·20	90	[9]
4	Synthetic high albite	0	100	0	8·151	12·862	7·115	93·65	116·45	89·98	[9]
5	Synthetic sanidine				8·353	12·983	7·162	90	116·17	90	Footnote 1
6	Synthetic sanidine				8·300	12·957	7·152	90	116·30	90	Footnote 1
7	Orthoclase	91	7	2	8·562	12·996	7·193	90	116·01	90	Spencer C [4, 11]
8	Intermediate microcline	86	13	1	8·578	12·960	7·211	90·30	115·97	89·13	Spencer U [1, 11]
9	Maximum microcline	100	0	0	8·589	12·963	7·223	90·62	115·95	87·73	Hugo KCl [9]
9M	Maximum microcline				8·585	12·958	7·223	90	115·95	90	Footnote 2, Hugo KCl [9]
10	Strained microcline	83	17	0	8·615	12·916	7·193	90·70	116·38	87·53	L29 [3]
11	Strained low albite	0	100	0	8·120	12·802	7·177	93·95	116·75	87·92	L29 [3]
12	Synthetic intermediate albite	0	100	0	8·160	12·810	7·152	93·95	116·48	88·60	219 [6]
13	Low albite	2	98	0	8·135	7·788	7·154	94·23	116·52	87·72	Spencer T [5, 11]
13A	Low albite				8·135	12·753	7·154	90	116·52	90	Footnote 2, [5, 11]
13P	Low albite				8·129	12·788	7·135	90	116·52	90	Footnote 2, [5, 11]
14	Low albite	1	98	1	8·141	12·785	7·159	94·26	116·59	87·68	191 [2]
15	Oligoclase	1	74	25	8·159	12·843	7·127	93·80	116·41	89·28	170 [2]
16	Low albite	2	98	0	8·208	12·839	7·173	93·86	116·25	87·52	F 101, 600 °C [6]
17	Oligoclase	3	75	22	8·199	12·849	7·129	93·43	116·20	88·80	F 36, 600 °C [7]
18	Andesine	4	59	37	8·171	12·862	7·119	93·59	116·30	89·68	5 [2]
19	Andesine	0	60	40	8·170	12·873	7·105	93·38	116·23	90·35	$An_{30}An_{50}$ [10]
20	Labradorite	1	45	54	8·169	12·862	7·108	93·58	116·22	89·81	81 [2]
21	Labradorite	1	41	58	8·180	12·870	7·109	93·52	116·20	90·04	96 [2]
22	Labradorite				8·177	12·862	7·108	93·60	116·29	89·74	sodic [8]
23	Labradorite				8·169	12·851	7·112	93·56	116·17	89·84	calcic [8]
24	Labradorite	0	31	69	8·175	12·865	7·102	93·50	116·14	90·31	45 [2]
25	Anorthite	0	7	93	8·179	12·873	7·090	93·21	115·97	91·11	116 [2] Footnote 3

Precision $\pm 0{\cdot}002$ Å and $\pm 0{\cdot}02°$ except for 10, 11, 16, 17: $\pm 0{\cdot}006$–8 Å and 0·05–8°.

Footnotes: (1) These parameters were invented taking into account thermal expansion data for albites (ref. [6]) and potassium feldspars (ref. [7]) and the effect of the substitution of K^+ for Na^+ in the feldspar framework.

(2) A for Albite twin with $b' = d_{010}$
P for Pericline twin with $a' = a \sin\gamma$, $c' = c \sin\alpha$, $\beta' = 180 - \beta$*
M for Albite and Pericline twins (M type), average of A and P.

(3) For convenience the c axis for anorthite was taken as 7 Å.

References

[1] Bailey & Taylor (1955)
[2] Bambauer, Eberhard & Viswanatham (1967)
[3] Brown *et al.* (1972)
[4] Cole, Sørum & Vennard (1949)
[5] Cole, Sørum & Taylor (1951)
[6] Grundy & Brown (1969)
[7] Grundy & Brown (1973)
[8] Nissen & Bollmann (1968)
[9] Orville (1967)
[10] Smith (1956)
[11] Spencer (1937)

Table 2. *Elastic stiffness coefficients, for axial system* 4 (10^{11} dyne cm^{-2} or 10^{10} Pascal)

(Orientation $\mathbf{z}_1 \perp \mathbf{z}_2$ and $\mathbf{z}_3 \parallel \mathbf{b}$, $\mathbf{z}_2 \parallel \mathbf{c}^*$)

	Feldspar	Composition Or	Ab	An	*A*	Ref.	c_{11}	c_{22}	c_{33}	c_{44}	c_{55}	c_{66}	c_{12}	c_{13}	c_{23}	c_{15}	c_{25}	c_{35}	c_{46}
A	Orthoclase	66·6	28·6		0	[1]	5·84	14·68	9·88	1·24	1·85	3·43	3·33	3·40	2·16	−1·07	−0·43	−1·30	−0·30
B	Microcline	64·9	26·6	3·6	1·00	[1]	5·96	15·81	10·49	1·39	2·03	3·70	3·62	3·60	2·85	−1·18	−0·57	−1·29	−0·26
C	Albite					no. 9 [2]	7·40	13·75	12·89	1·72	3·03	3·11	3·63	3·76	3·26	−0·91	−1·91	−1·91	−0·13
D	Oligoclase					no. 24 [2]	8·18	14·49	13·28	1·77	3·12	3·33	3·93	4·07	3·41	−0·50	−0·79	−1·85	−0·08
E	Labradorite					no. 56 [2]	9·89	17·20	14·14	1·99	3·41	3·76	5·21	4·41	3·66	−0·81	−0·51	−1·91	0·19
F	Isotropic					[3]	7·80	7·80	7·80	2·95	2·95	2·95	1·90	1·90	1·90	0	0	0	0

References [1] Ryzhova *et al.* (1965) – *A* and *B* contain considerable amounts of Ab and must be perthitic. They are thus already compositional averages. *A* indicates the 'triclinicity' of the potassium feldspar.
[2] Ryzhova (1964).
[3] The stiffnesses were calculated from those of an average glass (from Birch, Table 7-21 in Clark, 1966) where Young's modulus $E = 0{\cdot}7$ mbar and Poisson's ratio $= 0{\cdot}2$.

For the perthites, it is sufficiently good to assume domain compositions of pure K- and pure Na-feldspar: evidence for this will be given below, in § III.5 (actual compositions of exsolution pairs range from Or_0/Or_{100} to Or_{10}/Or_{75}). The more important differences concern symmetry and twinning. For trial purposes, we may divide perthites into four groups, depending on the symmetry of the domains (counting finely twinned triclinic domains as averaging to monoclinic). Writing the K-rich component first, they are as follows:

Group (1): Monoclinic/monoclinic
Group (2): Monoclinic/triclinic
Group (3): Triclinic/monoclinic
Group (4): Triclinic/triclinic.

The correlation of these groups with observed materials will be left to §§ III.4 and III.5. For the twinned materials, lattice parameters are constructed from the corresponding single-crystal lattice parameters as follows:

Albite law: a, d_{010}, c, 90°, β, 90°
Pericline law: $a \sin\gamma$, b, $c \sin\alpha$, 90°, 180–β*, 90°
Cross-hatched microline: average of the above two.

In the plagioclases, our state of knowledge is different for the three groups. For the *peristerites*, the composition pair is $Ab_{100}An_0/Ab_{75}An_{25}$ (Laves, 1954; Brown, 1960; Fleet & Ribbe, 1965; Ribbe, 1960) and the feldspar is highly ordered. For the *bytownites* (Huttenlocher intergrowth*) the compositional separation is less well known but may be considered to be $Ab_{33}An_{67}/Ab_{10-0}An_{90-100}$ (Nissen, 1968, 1972). For the *labradorites* (Bøggild intergrowth*) the situation is much less clear because of lack of data on the composition and state of order of the domains and the unknown role of potassium (Nissen, Eggmann & Laves, 1967; Nissen, 1971). In other words, in this series differences between the domains due to state of order may perhaps be as important as those due to composition. Moreover, it is known (Nissen, 1969) that in the bulk composition range An_{40}–An_{60} the lattice parameters vary erratically with composition, though in other parts of the plagioclase system they vary more smoothly. All that can be done in these circumstances is to try various combinations of sets of lattice parameters measured on materials in the right composition range.

Although the lattice parameters for very many homogeneous feldspars at room temperature have been measured, few high-temperature results are available. In general, room-temperature parameters for alkali feldspars and plagioclases have been used as no high-temperature measurements exist for the stiffness coefficients; two calculations using high-temperature parameters (directly measured or estimated from

* Term suggested by Smith (1972)

thermal expansions) have however been included for comparison.

The lattice parameters used in the calculations are given in Table 1. (The serial numbers in the Table do not refer to particular specimens, but are used in cross-reference to Table 3).

Stiffness coefficients for a series of seven alkali feldspars and five plagioclases have been measured at room temperature (Ryzhova, 1964; Ryzhova & Alexandrov, 1965; Ryzhova, Alexandrov & Belikov, 1969) and those used are reproduced in Table 2. Thirteen stiffness coefficients were measured for each of the two monoclinic feldspars and for each of the ten twinned triclinic ones treated as monoclinic: since the triclinic feldspars are very nearly monoclinic, the errors introduced by this simplification are probably not very great compared with the errors in the coefficients themselves; these are of the order of 3–10% depending on the coefficient (Alexandrov & Ryzhova, 1962; Ryzhova 1964; Simmons, 1964). The differences between coefficients for the plagioclases seem to vary systematically with composition, those rich in An being stiffer. It

Table 3. *Results of the calculations*

Exsolution	No.	Nature of domains†	Lattice parameters used‡		$c_{\alpha\beta}$	Calculated minimum φ	ϱ	h	k	l	W_{min} 10^4 J m^{-3}	W_{max}/W_{min}	P_{max}/P_{min}
Perthites group 1	1	Sa/H–Ab(P)*	1	4P*	A	90	98·5	$\overline{7{\cdot}9}$	0	1	360	6·7	14·6
(normal perthites)	2	Sa/H–Ab(A)*	1	4A*	A	90	99·5	$\overline{6{\cdot}8}$	0	1	420	6·0	12·8
	3	Or/L–Ab(P)	7	13P	A	90	100	$\overline{6{\cdot}4}$	0	1	480	5·2	11
	4	Or/L–Ab(A)	7	13A	A	90	99·5	$\overline{6{\cdot}8}$	0	1	600	4·6	9·3
	5	Or/L–Ab(A)	7	13A	C	90	101·5	$\overline{5{\cdot}7}$	0	1	620	5·6	9·3
	6	Or/L–Ab(A)	7	13A	F	90	97·5	$\overline{8{\cdot}4}$	0	1	380	9·6	9·3
	7	Sa/Sa	2	3	A	90	99	$\overline{7{\cdot}1}$	0	1	5·4	20	54
	8	Sa/Sa(HT)*	5	6	A	90	92·5	$\overline{25}$	0	1	8·9	4·4	10
Perthites group 2 (Braid perthites)	9	Or/L–Ab	7	13	A	124	107	$\overline{1}$	0·9	0·3	920	5·1	2·9
						123	137	$\overline{1}$	0·6	0·8	910	5·1	
	10	I–Mi(M)*/L–Ab	8M*	13	B	119·5	104·5	$\overline{1}$	1·2	0·3	107	4·7	2·9
	11	M–Mi(M)/L–Ab	9M	13	B	116·5	106·5	$\overline{1}$	0·8	0·3	113	4·6	2·9
Perthites group 3	12	I–Mi/L–Ab(A)	8	12A	B	79	98	$\overline{7{\cdot}8}$	$\overline{2{\cdot}5}$	1	350	6·7	15·3
(Diagonal association)	13	I–Mi/L–Ab(A)	8	12A	C	78	100	$\overline{6{\cdot}3}$	$\overline{2{\cdot}2}$	1	370	8·2	15·3
	14	M–Mi/L–Ab(A)	9	12A	B	69	97	$\overline{8{\cdot}5}$	$\overline{5{\cdot}6}$	1	170	22	32
	15	M–Mi/L–Ab(A)	9	12A	C	68	98	$\overline{7{\cdot}4}$	$\overline{5}$	1	210	18	32
	16	M–Mi/L–Ab(A)	10	11A	B	70	99·5	$\overline{6{\cdot}4}$	$\overline{3{\cdot}9}$	1	14	260	300
Perthites group 4	17	M–Mi/L–Ab	9	14	B	54	38	0·2	1	1·3	1420	2·6	3·4
(Plate-perthite)						88	96	$\overline{10{\cdot}4}$	$\overline{1{\cdot}1}$	1	1360	2·8	
						24	74	0·02	1	0·02	1470	2·6	
	18	M–Mi/L–Ab	9	14	C	77	88	28	12	1	1560	3·1	3·4
	19	M–Mi/L–Ab	9	14	F	52	100·5	0·8	1	$\overline{0{\cdot}2}$	1530	4·1	3·4
						86	66·5	1·8	0·3	1	1530	4·1	
Peristerites	20	L–Ab/L–Ol	14	15	C	169	74	0·2	$\overline{8}$	1·3	14·9	24	32
						103	119	$\overline{4}$	1·1	1·7	14·9	24	
	21	L–Ab/L–Ol	14	15	D	169	74	0·2	$\overline{8}$	1·3	15·2	25	32
						102	118	$\overline{4}$	1	1·7	15·2	25	
	22	L–Ab/L–Ol	14	15	F	172	81	0·3	$\overline{8}$	0·7	12	28	32
						100	111	$\overline{4}$	0·9	1·3	12	28	
	23	L–Ab/L–Ol(HT)*	16	17	C	175	68	0·5	$\overline{8}$	1·8	37	5·9	7·1
						96	130	$\overline{4}$	0·2	2·3	37	5·9	
Bytownites	24	L–Ab/An	24	25	E	92	114·5	$\overline{3}$	0·2	1·1	0·31	310	408
						171	75	0·1	$\overline{6}$	0·9	0·31	310	
	25	L–Ab/An	24	25	F	91	113	$\overline{3}$	0·2	1·0	0·22	340	408
						171	76	0·1	$\overline{6}$	0·8	0·22	340	
Labradorite	26	And/Lab	18	21	E	97	117·5	$\overline{3}$	0·5	1·2	1·0	26	25
						160	68	0·3	$\overline{4}$	0·9	1·0	26	
	27	And/Lab	19	20	E	97	116·5	$\overline{3}$	0·6	1·2	0·36	113	170
						179	87·5	0	12	$\overline{0{\cdot}2}$	0·36	113	
	28	Lab/Lab	22	23	E	63·5	80	$\overline{3}$	$\overline{3}$	$\overline{0{\cdot}6}$	0·02	380	220
						178	30	1·7	$\overline{4}$	3·5	0·02	380	

* P for Pericline twinned, A for Albite twinned, M for M-type twinned, HT for high-temperature.

† Abbreviations used H (High); L (Low); I (Intermediate); M (Maximum); Sa (Sanidine); Ab (Albite); Or (Orthoclase); Mi (Microcline); Ol (Oligoclase); And (Andesine); An (Anorthite); Lab (Labradorite).

‡ Cross references to Tables 1 and 2.

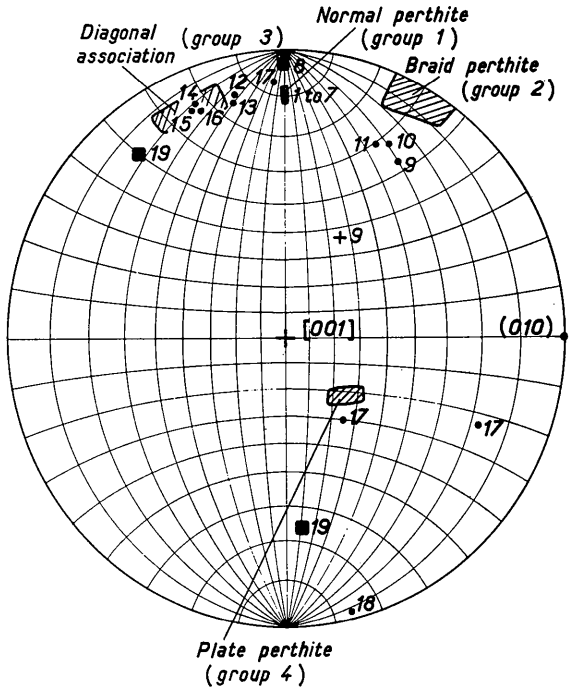

Fig. 5. Stereographic projection of the positions of the calculated energy minima compared with the observed exsolution boundaries for perthites (groups 1–4) – see Table 3. Symbols: – Physically reasonable input data, in good agreement ●, in poor agreement + with observations. Physically unreasonable input data ■.

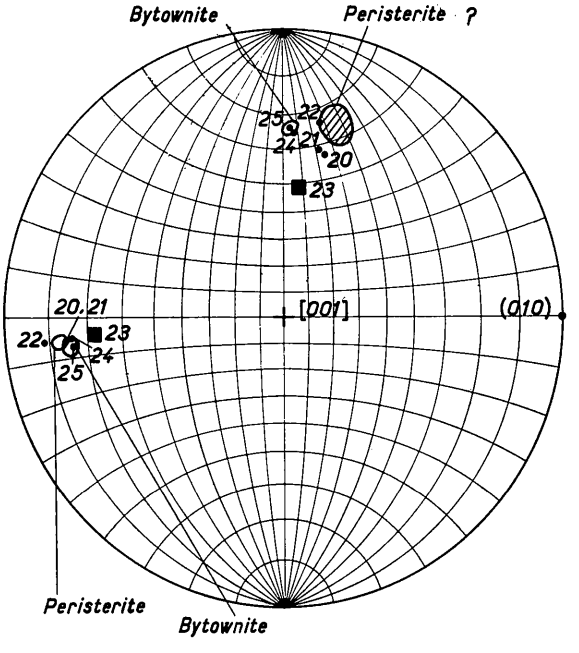

Fig. 6. Stereographic projection of the positions of the calculated energy minima compared with the observed exsolution boundaries for peristerites and bytownites. Same symbols as Fig. 5.

is not clear whether the differences within the K-rich feldspars are significant or not. In any case the feldspars are all so similar elastically that we felt justified in our calculations in using only one set of elastic coefficients for both compositional domains. No high-temperature measurements exist for the feldspars.

It is of interest to find the effect of elastic anisotropy. This can best be done by making comparison calculations with comparable isotropic stiffnesses. Table 2 therefore includes stiffness coefficients for a glass of composition similar to a feldspar.

3. *Results*

Table 3 gives the results of the calculations. The numbers in the second column are serial numbers used for reference in the text. Column 3 gives the character assumed for the domains. The corresponding choice of lattice parameters and stiffness coefficients is indicated in columns 4 and 5 by numbers and letters referring respectively to Tables 1 and 2.

For the perthites, all reasonable combinations of twins laws and symmetries were tried, each with reasonable choices of elastic stiffnesses. In addition, there were tests with isotropic elastic stiffnesses (6 and 19), strained parameters (16), less extreme compositions (7), and hypothetical high-temperature parameters (8). For the peristerites and bytownites, one choice of room-temperature lattice parameters was used for each, combined with different reasonable stiffnesses; in addition, there were trials using high-temperature parameters (23) and isotropic stiffnesses (22 and 25). For the labradorites, many calculations using reasonable compositional pairs were carried out, two representative examples are given (26 and 27). A third example (28) uses a combination of spacings deduced indirectly on the exsolution material, probably with lower accuracy (see § III.5). Calculations were carried out for values of φ and ϱ scanning over half of space in 10° steps, and in 1° steps in the neighbourhood of the minima.

The positions of these minima are given in terms of φ and ϱ, and also of the crystallographic indices (hkl) in column 6. They are plotted on stereograms in Figs. 5–7. The values of the minimum boundary strain energy $W_{\min}$ are given in column 7 and the ratios $W_{\max}/W_{\min}$ in column 8. The ratio of the pure strains $P_{\max}/P_{\min}$ on passing from one lattice to the other are given for comparison in column 9. They were calculated using a program written to determine the orientations of the thermal-expansion ellipsoid (Willaime, Brown & Perucaud, 1974).

We may call attention here to the occurrence of more than one minimum in certain perthites (examples 9,17–19) and in all the plagioclase exsolutions.

4. *Discussion of the calculated results*

This section deals with the results as related to the model and compares them with those of the model of Bollmann (Bollmann & Nissen, 1968; Nissen, 1972).

Mineralogical discussion, leading up to a comparison of calculated and observed results, will be given in § III.5.

It can be seen from the clustering of calculated orientations in Fig. 5 (Table 3, examples 1–19) that the empirical classification of the perthites into four groups has been justified. This allows us to treat the groups as entities in the following discussion. We shall show below that they are to be identified with observed series as follows:

Group (1), normal perthites, represented by moonstones
Group (2), braid perthites
Group (3), diagonal association
Group (4), plate perthites,
and we shall use these names where appropriate hereafter.

(a) Role of stiffness anisotropy and misfit anisotropy

The value of the minimum boundary energy, W_{min}, is sensitive to the difference in the parameters of the two domains and hence to the approximations of the model – assumption of complete coherence, no relaxation of the stresses away from the boundaries and use of the lattice parameters for the end compositions. It decreases as closer compositions are used. Comparisons between different exsolutions must therefore be made with caution.

On the other hand, the ratio W_{max}/W_{min} is nearly the same for extreme parameters and intermediate parameters. This ratio can thus be compared for the different calculations. It gives a measure of the variation of the boundary elastic energy with boundary orientation. The ratio P_{max}/P_{min} gives a measure of the misfit anisotropy (see § II.4). The anisotropy of the elastic stiffness coefficients is of the order of 2·5 in the feldspars – the ratio c_{22}/c_{11} ranges from about 2 to 3. It can be seen that in some cases the stiffness anisotropy is negligible compared to the misfit anisotropy; in others, they are of the same order of magnitude.

When $P_{max}/P_{min} \geq 10$ (bytownites, peristerites, normal perthites, diagonal association) the stiffness anisotropy is negligible compared with the misfit anisotropy, hence the influence of the elastic stiffnesses on the orientation of the plane of minimum energy is small. The use of isotropic elastic stiffnesses (Table 2, *F*) in the calculations only changes the orientation by 1° for the bytownites (Table 3, no. 25) and by about 10° for the peristerites (no. 22). *A fortiori* the use of the elastic stiffnesses for a feldspar of composition different from that of the bulk composition has even less effect on the orientation of the boundary plane. For the peristerites, the orientation varied less than 1° on using the stiffnesses for albite (*C*) or those for oligoclase (*D*) (Table 3, no. 20 and 21). Thus, the use of the elastic stiffnesses for labradorite (Table 2, *E*), those for bytownite not having been measured, will not significantly affect the results for the bytownites.

The large misfit anisotropy in these cases justifies the use of the optimal-phase-boundary theory for the calculation of the orientation of the exsolution boundary. The results of Nissen (1972) for these exsolutions are in good agreement with our results (Willaime & Brown, 1972 and Table 3). For comparison, we have done a calculation (Table 3, no. 16) with the lattice parameters used by Nissen in the case of the diagonal association, which were those measured on a specimen after partial relaxation (Brown, Willaime & Guillemin, 1972); it gave $P_{max}/P_{min} = 300$.

For braid and plate perthites, on the contrary, the deformation is quasi-isotropic; the ratio P_{max}/P_{min} is 2·9 and 3·4 and is of the same magnitude as the stiffness anisotropy. The orientation of the calculated boundary plane is very sensitive to variations in the

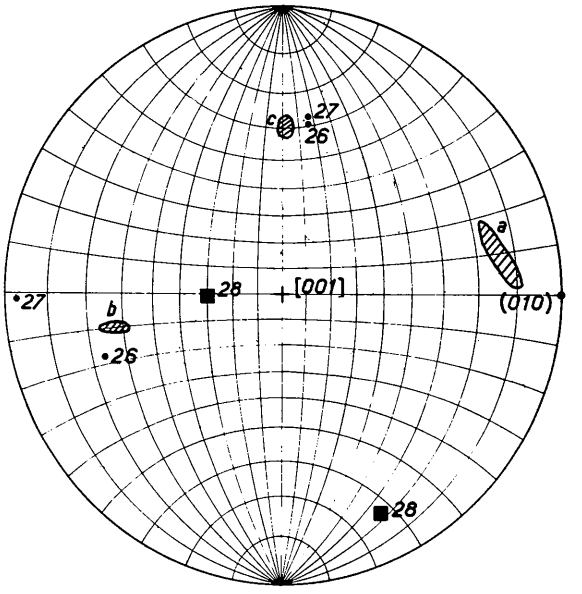

Fig. 7. Stereographic projection of the positions of the calculated energy minima compared with the observed exsolution boundaries for labradorites. Same symbols as Fig. 5.

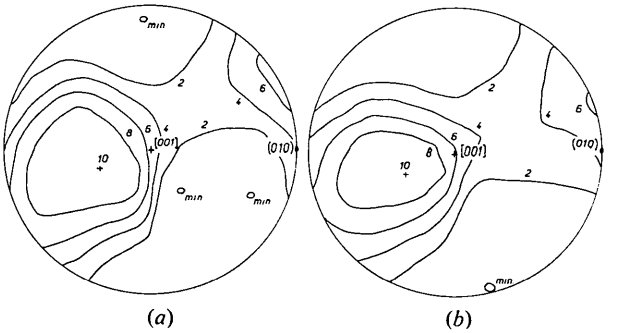

(*a*) (*b*)

Fig. 8. Stereographic projection of the contours of equal boundary elastic energy for plate perthite: (*a*) elastic stiffnesses for microcline (Table 3, no. 17); (*b*) elastic stiffnesses for albite (Table 3, no. 18). The zones of low energy are very spread out and are almost the same for both. The minima are not in the same places.

elastic stiffnesses. In the case of the plate perthites the stiffnesses for microcline (Table 2, *B*) gave three directions of minimum energy [Fig. 8(*a*), Table 3, no. 17]. On using the elastic stiffnesses of albite (*C*) only one of these minima remained (Table 3, no. 18) but rotated by 15° compared with the positions obtained with *B*; in the directions corresponding to the other two minima, the boundary elastic energy remained low, but was not a minimum [Fig. 8(*b*)]. Using isotropic elastic stiffnesses, two minima were obtained which bear no relation to the observed boundaries in the plate perthites (Table 3, no. 19). Because of the quasi-isotropy of the strain, the optimal-phase-boundary model cannot give results in accordance with observations. In fact, Nissen (1972) found no minima corresponding to plate perthites for the relative orientation given by Laves & Soldatos (1962).

For a perthite with domains of orthoclase and untwinned low albite (Table 3, no. 19) the calculated orientations corresponding to the energy minima were compared with the results of Bollmann & Nissen (1968) using the same lattice parameters: they are completely different, because the stiffness anisotropy is as important as the misfit anisotropy.

(b) The effect of relaxation of stresses away from the boundary

In the discussion of the coherent elastic model (§ II. 3*a*) it was shown that unstressed lattice parameters should be used for the calculation. The results obtained using parameters deformed through coherence stresses are a complicated function of the elastic energy and the relaxation energy. To examine the effect empirically, a calculation (no. 16) was carried out using parameters measured on a crystal with partial relaxation of the coherency stresses neglecting the zone of rapid change near the boundary, and the result was compared with calculations (nos. 12–15) using different unstressed parameters. It can be seen from Fig. 5 that the orientations are very close to one other; the difference between nos. 16 and 14, with similar stiffnesses, is about 4°.

One can conclude that the energy corresponding to the relaxation of stresses and the coherent-boundary elastic energy vary in the same way with the orientation of the boundary. This justifies *a posteriori* the simple model which neglects relaxation.

(c) Use of high-temperature lattice parameters

Calculations have been carried out using parameters at 600 °C, a temperature near the supposed exsolution conditions. For the perthites (Table 3, no. 8 – invented parameters) the calculated minimum is displaced by about 8°. For the peristerites (no. 23) the deviation is about 10–15°. As the value of P_{max}/P_{min} falls from 54 to 10 in the first-named example, and from 32 to 7·1 in the second, it is necessary to use the correct high-temperature elastic stiffnesses. In these two cases, the use of room-temperature lattice parameters and stiffnesses gives better results.

(d) Errors in the input parameters

Errors in the input data (compositions used, lattice parameters and elastic stiffnesses) will lead to uncertainty in the calculated exsolution boundary. The effect of errors in lattice parameters was examined by calculations in which the parameters were varied one at a time by the magnitude of the experimental error. There will be the greatest effect on the orientation when the parameter differences are small and the misfit anisotropy is small. All cases were examined and the calculated differences of orientation are given in Table 4.

(e) The values of the energy minima

In the cases of the peristerites, the labradorites and the bytownites as we noted in § III.3, our calculations gave two directions for the optimal boundary. In all these calculations the values of W_{min} are equal within 1 %, for orientations calculated with an error of 0·5°. Fig. 9 shows a stereographic projection of the contours of equal boundary elastic energy in a case with two minima (bytownite).

The theory offers no explanation, at this stage of approximation, as to why one minimum rather the other should be chosen in any given case.

These double minima correspond to the case, where the quadric associated with the pure-strain tensor is a hyperboloid* (see § II.4) and the parameter *P* is a

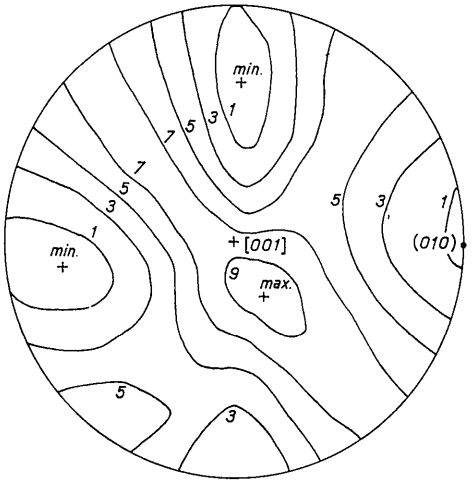

Fig. 9. Stereographic projection of the contours of equal boundary elastic energy for bytownite (Table 3, no. 24). Two minima of very nearly equal energy are clearly visible. The labradorites and peristerites also show two minima.

* In the three cases considered this result could be predicted without any calculation, since **a** and **b** vary in the opposite way to **c**. But the fact that all three parameters may vary in the same way is no proof of the existence of a single maximum; angular variations may be very important and a direction may exist (other than **a**, **b** or **c**) for which the sign of a variation is opposite to that of **a**, **b** and **c**.

Table 4. *Calculated and observed orientations*

	Calculated orientations					Observed orientations						
	No. of min.	Ref. of Table 3	Indices h	k	l	Indices h	k	l	References	Comments	$\Delta\theta$	Error*
Moonstone (perthite, group 1)		1—5	$\overline{5{\cdot}7}$ to $\overline{7{\cdot}9}$	0	1	$\bar{6}$ to $\bar{8}$	0	1	Bøggild (1924)	Precise work	$<0{\cdot}5°$	$<0{\cdot}5°$
Braid perthite (group 2)		10, 11	$\bar{1}$ to $\bar{1}$	0·8 1·2	0·3 0·3	$\bar{1}$ to $\bar{1}$	1	0 0·1	Goldich & Kinser (1939) Ramberg (1972)		10–15°	2°
Diagonal association (group 3)		12–15	$\overline{7{\cdot}8}$ to $\overline{7{\cdot}4}$	$\overline{2{\cdot}5}$ $\bar{5}$	1 1	$\bar{6}$ to $\bar{6}$	$\bar{3}$ $\bar{6}$	1 1	Brown *et al.* (1972)	Few samples	~0°	$<0{\cdot}5°$
Plate perthite (group 4)	1st	17	$0{\cdot}2$	1	1·3	~0	1	1	Laves *et al.* (1962)	Albite platelets imprecise	5°	1°
	2nd	17	$\overline{10{\cdot}4}$	$\bar{1}$	1	~$\bar{6}$	0	1			3°	1°
	3rd	17	0	1	0					Uncertain		1°
Peristerite	1st	20, 21	0·2	$\bar{8}$	1·3	0 to 1	$\bar{8}$ $\bar{21}$	1 2	Bøggild (1924)	Precise work	3–5°	5°
	2nd	20, 21	4	1	1·7	$\bar{4}$	1	1?	Korekawa *et al.* (1970)	Imprecise work	3–5°	5°
Bytownite†	1st	24	$\bar{3}$	0·2	1·1	$\bar{3}$	0	1	Nissen (1972)		2–3°	7°
						$\bar{3}$	0	2	Nord *et al.* (1972)			
	2nd	24	0·1	$\bar{6}$	0·9	0	$\bar{6}$	1	Jäger *et al.* (1955); Nissen (1972); Nord *et al.* (1972)		1·2°	
Labradorite†	1st	27	0	12	$\overline{0{\cdot}2}$	$\bar{1}$ to $\bar{9}$	12 33	1 4	Bøggild (1924)	Many observed	15°	~20°
									(*a*)			
		26	0·3	$\bar{4}$	0·9	0 to $\bar{1}$	$\bar{4}$ $\overline{22}$	1 7	(*b*)	Some observed	7°	24°
	2nd	26, 27	$\bar{3}$	0·5	1·2	$\bar{3}$	0	1	(*c*)	Few observed	5–7°	13°

* Estimated error due to lattice parameter uncertainty.
† With the c parameter taken as 7 Å.

minimum for two different orientations with a value of $P=(S_2^E)^2$. The boundary elastic energy is a minimum for orientations close to those where P is a minimum,

$$W^E \simeq \tfrac{1}{2}[c_{22}(S_2^E)^2 + c_{23}S_2^E S_3^E + c_{24}S_2^E S_4^E + c_{25}S_2^E S_5^E] \ .$$

In this expression the term $c_{22}(S_2^E)^2$ is the most important and has the same value for the two orientations for which P is a minimum. For the two directions of minimum boundary energy, the elastic anisotropy makes all the terms very slightly different. This explains why the values of $W_{\min}$ are almost equal.

When the elastic anisotropy is not negligible compared to the strain anisotropy (braid perthites, plate perthites), the multiple minima $W_{\min}$ differ by up to 6%. In such cases, the elastic anisotropy plays a role in determining the number of minima (1 to 3 instead of 2), their orientations and their values.

5. *Comparison of the observed and calculated exsolution boundaries*

It is necessary to review the experimental evidence for each group of exsolutions separately before the calculated orientations can be compared with the observed. It should be stressed at this point that only the normal perthites are considered by us to be a product of primary exsolution, the other types being considered to have formed from normal perthites by rearrangement (Brown, Willaime & Guillemin, 1972 and unpublished results).

(*a*) *Normal perthites* [*Group* (1) *perthites. See Fig.* 5]

These are well known from the work of Bøggild (1924) on a series with fine-scale lamellations – the moonstones. It is generally accepted that the K-rich domains and the Na-rich domains are monoclinic or finely-twinned triclinic. The measured range of ϱ values (known with good precision) is 98·5–101·8°. The calculated range, 97·5–102° for physically reasonable input, agrees excellently with the observed. The calculated values show no significance associated with the character of the domains or the twinning; a pair comprising two sanidines of intermediate composition gives essentially the same value of ϱ as pairs comprising pure sanidine or orthoclase with high or low albite twinned according to the Albite or the Pericline law.

(*b*) *Braid perthites* [*Group* (3) *perthites. See Fig.* 5]

These are less well known than the previous group. They have been studied chiefly by Goldich & Kinser (1939) and Ramberg (1972) using mainly optical microscopy. Our electron-optical results are extremely complex and are not discussed here.

In coarse braid perthites, albite occurs in large zigzag lamellae in a cross-hatched microcline matrix. The albite is coarsely twinned according to the Albite law, each twin composition plane occurring where the lamella changes direction (Goldich & Kinser, 1939, p. 411, Plates I*A* and II*A*). The boundary plane is nearly parallel to (110) ($\varphi \simeq 60°$, $\varrho = 90°$) (measured from Goldich & Kinser, 1939) or, to $(\bar{8}61)$ ($\varphi \simeq 117°$, $\varrho \simeq 95°$) in braid microperthite (Ramberg, 1972). Contrary to the observations of Ramberg (1972) we found that braid microperthite from the same localities is not in diagonal association (unpublished work).

A calculation (Table 3, no. 9) using the parameters of orthoclase and twinned low albite gave two minima, one near the observed orientation ($\sim 10°$), the other farther ($\sim 40°$). Two further calculations (nos. 10–11) using the average monoclinic parameters for Albite- and Pericline-twinned intermediate and maximum microcline gave one minimum near the observed orientation (~ 10–$15°$).

(*c*) *Diagonally associated perthites* [*Group* (3) *perthites. See Fig.* 5]

Smith & MacKenzie (1959) studied a cryptoperthite whose X-ray diffraction patterns presented a double spot for triclinic K-rich domains, very slightly rotated from the albite twin position, and Albite-twinned albite spots; they called this the diagonal association. An electron-optic study (Brown, Willaime & Guillemin, 1972) showed that the K-rich domains occur in large zigzags, each orientation of the zigzag corresponding to one of the rotated twins. The boundary-plane orientation between these K-rich domains and the finely Albite-twinned triclinic Na-rich domains varies from $(\bar{6}61)$ to $(\bar{6}31)$ ($\varphi \simeq 60$–$75°$ and $\varrho \simeq 100°$).

This kind of perthite differs from normal perthites because, on the one hand, the K-rich domains are triclinic instead of monoclinic, and on the other hand, the boundary plane is nearly parallel to $(\bar{6}61)$ instead of $(\bar{6}01)$.

The calculated values for the boundary lie within the observed ranges (Brown, Willaime & Guillemin, 1972). The value of φ is 69° for (maximum-microcline)/(low albite) (no. 14–15), 79° for (intermediate-microcline)/(low-albite) (no. 12–13) and 90° for (orthoclase)/(low albite)/(normal perthite). This suggests that the boundary migrates from $(\bar{6}01)$ in normal perthites towards $(\bar{6}61)$ as the potassium feldspar becomes more and more oblique; from this the formation of the diagonally associated perthites can be explained (Brown & Willaime, 1973).

(*d*) *Plate perthites* [*Group* (4) *perthites. See Fig.* 5]

The plate perthites have been studied in detail by Laves & Soldatos (1962) from the point of view of the mutual orientation of the two lattices after relaxation. These perthites consist of triclinic domains, whose boundary planes are mainly (011) ($\varphi \simeq 45°$; $\varrho \simeq 30°$) for the plates and near $(\bar{6}01)$ ($\varphi \simeq 90°$; $\varrho \simeq 98°$) for the film perthite which persists (see photos in Laves & Soldatos). On the published photos one can see other boundaries whose orientations are difficult to determine. The calculations give three minima for the

elastic-boundary energy; the orientations of two of them are in good agreement with the main observed boundaries.

(*e*) *Peristerites* (*see Fig.* 6)

The peristerites have been well studied and the prominent schiller plane is near (0$\bar{8}$1) with a few near (1,2$\bar{1}$,2) (Bøggild, 1924; Brown, 1960).

Nissen (in Korekawa, Nissen & Philipp, 1970) found a second lamellar structure in a very fine peristerite which made an angle of 75–80° in (001) with the first. If the one of these is (0$\bar{8}$1), the second could well be ($\bar{4}$11) since the angle between their traces in (001) is 77–78°.

The first calculated minimum is close to the main observed orientation and agrees within 3–5°. The second calculated minimum has indices near ($\bar{4}$11) to ($\bar{4}$12); if the suggested identification of the second observed orientation is correct, there is agreement here too.

(*f*) *Bytownites* (*see Fig.* 6)

In the bytownites no schiller has been reported, but thin lamellae are visible under the microscope in basic plagioclases making an angle of 17° with (010) and having indices near (0$\bar{6}$1) (Jäger & Huttenlocher, 1955). Such lamellae have been observed under the electron microscope (Nissen, 1968, 1971). Two lamellar structures have been reported near (0$\bar{6}$1) and ($\bar{3}$01) by Nissen (1971) and near (0$\bar{6}$1) and ($\bar{2}$01) by Nord, Heuer & Laly (1973), where the indices are expressed with $c=$ 7 Å. The two calculated minima lie within 3° of the two observed orientations found by Nissen and slightly farther from the second direction ($\bar{2}$01) found by Nord *et al.* (1973).

(*g*) *Labradorites* (*see Fig.* 7)

The labradorites present a problem because two lattices cannot be distinguished by normal X-ray techniques, though Nissen & Bollmann (1968) observed doubled Kikuchi lines in electron diffraction patterns. It is clear that the more similar the input parameters are, the greater will be the effect of uncertainties on the calculated boundaries. There are three observed ranges of schiller directions shown in Fig. 7 taken from Bøggild (1924).

(*a*) Many in a broad range of 15° from near ($\bar{1}$,12,1) to ($\bar{9}$,33,4);

(*b*) Some between (0$\bar{4}$1) and ($\bar{1}$,2$\bar{2}$,7) and

(*c*) a few near ($\bar{3}$01). In some specimens two directions are visible.

It can be seen that Bøggild's groups (*a*) and (*b*) are within 10–35° of (010) and (*c*) close to the common minimum near ($\bar{3}$01).

The calculated minima fall into two groups, those nearest to (010) and those nearest to ($\bar{3}$01). For calculations using parameters for natural plagioclases (nos. 26–27) one minimum was found close to group (*c*) and a second less than 20° either from group (*a*) (no. 27) or from group (*b*) (no. 26).

One input pair (no. 28) gave more aberrant results for which the angular differences between observed and calculated orientations are 35 and 45°. These lattice parameters taken from Nissen (1972) were obtained from a natural specimen using doubled Kikuchi lines and are probably of lower precision.

The comparison of calculated and observed results is summed up in Table 4. The calculated results shown are selected from those in Table 3 as representative of the physically realistic input combinations for each group. The difference $\Delta\theta$ between calculated and observed orientations, and the errors estimated as described in § III.4*d* are also given. It is interesting to note that the calculated errors are largest where the disagreement between the observed and calculated orientations are greatest.

IV. Conclusion and comments

On the whole, the agreement between calculated and observed orientations must be regarded as excellent. For five of the seven distinct systems used for comparison, the angular differences between calculated and observed orientations were very small; for a sixth, (the braid perthites) they were moderately small. Only for the labradorites, which are very sensitive to uncertainties in the input parameters, could the agreement be regarded as doubtful. In nearly all cases where two or more minima were predicted, there is some experimental evidence of a second boundary in the correct orientation. These results are considered to be a justification of the model and of its approximations: – use of unstressed room-temperature lattice parameters and elastic stiffnesses instead of those for the conditions of exsolution, and the neglect of relaxation. The use of high-temperature lattice parameters with room-temperature stiffnesses gave less good results. The high-quality of the results indicates that the relaxation energy varies as a function of orientation in the same way as the coherent-boundary energy.

The calculations are of heuristic value both because they draw attention to areas requiring further study and also because they may enable a genetic theory of the formation of the exsolutions to be elaborated.

The model was applied to the feldspars because they have several exsolution domains and because there are few symmetry contraints. It could be applied to other problems such as the pyroxenes which are much simpler – Morimoto & Tokonami (1969) carried out approximate calculations for four directions – or to the amphiboles for which a simplified 0-lattice model has been applied (Robinson, Jaffe, Ross & Klein, 1971).

The authors are grateful to M. Gandais for fruitful discussions and M. C. Pérucaud for help with the calculations. We thank D. B. Stewart and J. V. Smith

for carefully reading the typescript. We thank Helen D. Megaw for many suggestions, which greatly helped in clarifying the text.

References

ABERDAM, D. (1965). *Sci. Terre, Nancy*, **6**, 1–76.

ABERDAM, D. & KERN, R. (1962). *C. R. Acad. Sci. Paris*, **255**, 734–736.

ALEXANDROV, K. S. & RYZHOVA, T. V. (1962). *Izv. Akad. Nauk. SSSR, Ser. Geophys.* pp. 186–189.

BAILEY, S. W. & TAYLOR, W. H. (1955). *Acta Cryst.* **8**, 621–632.

BAMBAUER, H. U., EBERHARD, E. & VISWANATHAN, K. (1967). *Schweiz Miner. Petrogr. Mitt.* **47**, 351–364.

BØGGILD, O. B. (1924). *Kgl. Danske Vidensk. Selsk. Math. Fys. Medd.* **6**, 1–79.

BOLLMANN, W. (1967). *Phil. Mag.* **16**, 363–383.

BOLLMANN, W. (1970). *Crystal Defects and Crystalline Interfaces*. Berlin: Springer.

BOLLMANN, W. & NISSEN, H. U. (1968). *Acta Cryst.* A**24**, 546–557.

BONNET, R. & DURAND, F. (1972). *Mater. Res. Bull.* **7**, 1045–1060.

BROWN, W. L. (1960). *Z. Kristallogr.* **113**, 330–344.

BROWN, W. L. & WILLAIME, C. (1973). NATO Report. In MACKENZIE & ZUSSMAN (1973).

BROWN, W. L., WILLAIME, C. & GUILLEMIN, C. (1972). *Bull. Soc. fr. Miner. Crist.* **95**, 429–436.

CADORET, R. & DELAVIGNETTE, P. (1969). *Phys. Stat. Sol.* **32**, 853–865.

CAHN, J. W. (1961). *Acta Met.* **9**, 795–801.

CAHN, J. W. (1962). *Acta Met.* **10**, 179–183.

CAHN, J. W. (1968). *Trans. Met. Soc. AIME*, **242**, 166–180.

CLARK, S. P. (1966). *Handbook of Physical Constants, Geol. Soc. Amer. Mem.* **97**.

COLE, W. F., SÖRUM, H. & KENNARD, O. (1949). *Acta Cryst.* **2**, 280–287.

COLE, W. F., SÖRUM, H. & TAYLOR, W. H. (1951). *Acta Cryst.* **4**, 20–29.

FLEET, S. G. & RIBBE, P. H. (1965). *Miner. Mag.* **35**, 165–176.

GOLDICH, S. S. & KINSER, J. H. (1939). *Amer. Min.* **24**, 407–427.

GRUNDY, H. D. & BROWN, W. L. (1969). *Miner. Mag.* **37**, 156–172.

GRUNDY, H. D. & BROWN, W. L. (1973). NATO report. In MACKENZIE & ZUSSMAN (1973).

JÄGER, E. & HUTTENLOCHER, H. (1955). *Schweiz. Min. Petrogr. Mitt.* **35**, 199–207.

KOREKAWA, M., NISSEN, H. U. & PHILIPP, D. (1970). *Z. Kristallogr.* **131**, 418–436.

LAVES, F. (1952). *J. Geol.* **60**, 549–574.

LAVES, F. (1954). *J. Geol.* **62**, 409–411.

LAVES, F. & SOLDATOS, K. (1962). *Z. Kristallogr.* **117**, 218–226.

MCCONNELL, J. D. C. (1973). NATO Report. In MACKENZIE & ZUSSMAN (1973).

MACKENZIE, W. S. & ZUSSMAN, J. (1973) *Feldspar*. Manchester Univ. Press.

MORIMOTO, N. & TOKONAMI, M. (1969). *Amer. Min.* **54**, 1101–1117.

NISSEN, H. U. (1968). *Schweiz. Miner. Petrogr. Mitt.* **48**, 53–55.

NISSEN, H. U. (1969). *Schweiz. Miner. Petrogr. Mitt.* **49**, 491–498.

NISSEN, H. U. (1971). *Naturwissenschaften*, **58**, 454.

NISSEN, H. U. (1972). Unpublished work.

NISSEN, H. U. & BOLLMANN, W. (1968). *4th European Reg. Conf. Electron Microscopy, Rome.*

NISSEN, H. U., EGGMANN, H. & LAVES, F. (1967). *Schweiz. Min. Petrogr. Mitt.* **47**, 289–302.

NORD, G. L., HEUER, A. H. & LALLY, J. S. (1973). NATO Report. In MACKENZIE & ZUSSMAN (1973).

ORVILLE, P. M. (1967). *Amer. Min.* **52**, 55–86.

OWEN, D. C. (1973). NATO Report. In MACKENZIE & ZUSSMAN (1973).

OWEN, D. C. & MCCONNELL, J. D. C. (1971). *Nature, Lond.* **230**, 118–119.

RAMBERG, I. B. (1972). *Lithos*, **5**, 281–306.

RIBBE, P. H. (1960). *Amer. Min.* **45**, 626–644.

ROBINSON, P., JAFFE, H. W., ROSS, M. & KLEIN, C. (1971). *Amer. Min.* **56**, 909–939.

RYZHOVA, T. V. (1964). *Izv. Akad. Nauk. SSSR, Ser. Geophys.* pp. 1049–1051.

RYZHOVA, T. V. & ALEXANDROV, K. S. (1965). *Phys. Zemli.* pp. 98–102.

RYZHOVA, T. V., ALEXANDROV, K. S. & BELIKOV, B. P. (1969). *Zap. Vses. Mineral. Obshchestva. Ser.* II, 1st ed. **98**, 41–54.

SIMMONS, G. (1964). *J. Geophys. Res.* **69**, 1117–1121.

SMITH, J. V. (1956). *Miner. Mag.* **31**, 47–68.

SMITH, J. V. (1961). *Amer. Min.* **46**, 1489–1493.

SMITH, J. V. (1972). *J. Geol.* **80**, 505–525.

SMITH, J. V. & MACKENZIE, W. S. (1959). *Amer. Min.* **46**, 1169–1186.

SPENCER, E. (1937). *Miner. Mag.* **24**, 453–494.

VISWANATHAN, K. (1968). *Schweiz. Miner. Petrogr. Mitt.* **48**, 803–814.

VISWANATHAN, K. (1973). NATO Report. In MACKENZIE & ZUSSMAN (1973).

WILLAIME, C. & BROWN, W. L. (1972). *C. R. Acad. Sci. Paris, Sér. D*, **275**, 627–629.

WILLAIME, C., BROWN, W. L. & PERUCAUD, M. C. (1974). *Amer. Min.* In the press.

WILLAIME, C. & GANDAIS, M. (1972). *Phys. Stat. Sol. (a)*, **9**, 529–539.

WRIGHT, T. L. & STEWART, D. B. (1968). *Amer. Min.* **53**, 38–87.